Please cite as: *Hsu MH, Lin SH, Fu JC, Chung SF, Chen AS. (2010) Longitudinal stage profiles forecasting in rivers for flash floods, Journal of Hydrology, 388 (3-4), 426-437, DOI:10.1016/j.jhydrol.2010.05.028.*

Longitudinal Stage Profiles Forecasting in Rivers for Flash Floods

Ming-Hsi Hsu[a,1], Shu-Horng Lin[a], Jin-Cheng Fu[b], Shih-Feng Chung[a], Albert S. Chen[c]

[a] Department of Bioenvironmental Systems Engineering, National Taiwan University, 1 Roosevelt Road, Sec. 4, Taipei 10617, Taiwan, ROC

[b] National Science & Technology Center for Disaster Reduction, 9F., 200 Beisin Road, Sec. 3, Sindian City, Taipei County 231, Taiwan, ROC

[c] Centre for Water Systems, College of Engineering, Mathematics and Physical Sciences, University of Exeter, Harrison Building, North Park Road, Exeter, EX4 4QF, UK

Abstract

A flash flood routing model with artificial neural networks predictions was developed for stage profiles forecasting. The artificial neural networks were used to predict the 1-3 hour lead time river stages at gauge stations along a river. The preditions were taken as interior boundaries in the flash flood routing model for the forecast of longitudinal stage profiles, including un-gauged sites of a whole river. The flash flood routing model was based on the dynamic wave equations with discretization processes of the four-point finite difference method. Five typhoon events were applied to calibrate the rainfall-stage model and other three events were simulated to verify the model's capability. The results revealed that the flash flood river routing model incorporating with artificial neural networks can provide accurate river stages for flood forecasting.

Keywords: Stage Profiles forecasting; Flash Flood Routing; Artificial Neural Networks

[1] Corresponding Author. Address: Department of Bioenvironmental Systems Engineering, National Taiwan University, 1 Roosevelt Road, Sec. 4, Taipei 10617, Taiwan, ROC; Tel: +886-2-33663468; Fax: +886-2-23631209; e-mail: mhhsu@ntu.edu.tw

Please cite as: *Hsu MH, Lin SH, Fu JC, Chung SF, Chen AS. (2010) Longitudinal stage profiles forecasting in rivers for flash floods, Journal of Hydrology, 388 (3-4), 426-437, DOI:10.1016/j.jhydrol.2010.05.028.*

1. Introduction

Flooding is the most frequent natural disaster that causes heavy losses to life and property in the world. In Taiwan, tropical storms typically result in disastrous flash floods in a short time because of steep terrains and intense rainfall. Experiences showed that the combination of structural and non-structural measures can significantly reduce the flood risk (Sabino et al., 1999). The flood forecasting and warning system based on hydrological and/or hydraulic models plays an important role in flood risk management. During flood emergency operations, the managers rely on accurate flood forecasting that is analyzed within limited time to take proper actions for reducing damages. Hsu et al. (2000) built a flash flood routing model, based on the dynamic wave theory of unsteady flow in open channels, and successfully forecasted the flood flows in the Tanshui River Basin.

Incorporating observation data with a flood routing model to improve the accuracy of forecasting is a challenging task for hydraulic engineers. Several studies have discussed how to apply observed data in the works of real-time river flow computation. Ford (2001) established a practical flood-warning decision support system (FW-DSS) for Sacramento County in California. The FW-DSS includes various modules that can routinely measure the rainfall depths and the water levels, transmit the real-time observations to the operation center, execute the flood forecasting model, archive the data and display these information. The system can also automatically detect the flood threats and report to emergency managers. With the remarkable development of computing technology in recent years, the dynamic routing models have been widely utilized for flood forecasting (Saavedra et al., 2003). Hsu et al. (2003) used real-time observed river stages as the internal boundary

conditions to adjust the computed river flow conditions in a flood forecasting model, which adopted the least-squares method to improve the model accuracy for solving over-determined problems. Later, Hsu et al. (2006) further developed the technique of updating time-varying roughness in channels, by using a stochastic-dynamic and least-squares method, to obtain better predictions in flood forecasting. Littlewood et al. (2007) coupled with the rainfall forecasts to the input of observed raifall to improve the predicting accuracy of stream flow.

The recent advances in artificial intelligence, data mining and computer hardware have enhanced computational power to forecast river stages. Campolo et al. (1999) developed a neural network model to forecast river stage by using current rainfall and stage information. Chang et al. (2002) implemented a real-time recurrent learning algorithm in artificial neural networks (ANN) that adopted time variate characteristics in hydrological processes to forecast the stream flows. Rajurkar et al. (2004) used a simple linear black box model with ANN for daily flow forecasting during flood events. A multilayer feed-forward trained with a back-propagation algorithm has been conducted for flow prediction in Morocco (Riad et al., 2004). Diamantopoulou et al. (2006) developed a time delay ANN model that adopted Kalman's learning rule to modify weights for forecasting daily flows. Chiang et al. (2007) combined gauge observations and satellite-derived precipitation in a recurrent neural network model to simulate the hydrologic responses from various rainfalls.

The data-driven method like ANN restricts that the stages are predictable at the gauge sites only. The longitudinal river stage profiles forecasting along rivers are not available yet. In Taiwan, many towns situated by rivers are vulnerable to flash flooding but no gauge nearby is available for the data-driven forecasting. The aim of the study was to forecast the longitudial stage profiles along rivers by adopting the

data assimilation technique. We adpoted the ANN stage predictions at gauges as the updated interior boundary conditions for stage forecasting in the flash flood routing model (FFRM). With the improved internal boundary conditions, the coupled FFRM and ANN model (FFRM-ANN) can provide reliable forecasting of stage profiles and discharges of a river system, including the gauged and the unmeasured sites along the rivers.

2 Model Descriptions

2.1 Artificial Neural Network (ANN)

An ANN is a computational methodology system based on human brain structure and functions that solves problems by applying information acquired from experience to new problems and case scenarios (Simon, 1999). In recent years, ANN provides an alternative approach for forecasting in many research fields. ANN models are usually classified as two broad categories, feed-forward (FF) networks and feed-backward (FB) networks, according to the pattern of data flow of the model input information within the architecture. The basic structure of an ANN model consists of three layers: the input layer, where the data are introduced to the ANN, one or more hidden layers, where the data are processed, and the output layer, where the results of ANN are produced (Sudheer, 2002). Each layer consists of a set of nodes that are similar to human's brain neuron, each node in a layer takes all the nodes in the previous layers as inputs, performs a calculation process, and provides its output as input to all nodes in the next layer.

The signal is unidirectional without feedback cycles between nodes in a FF network (Campolo, 1999). A FF network with an error-back-propagation (EBP)

algorithm is commonly used to reduce the error against the observed data. We predicted, in the study, river stages at gauge stations along the river using a FF neural network, which was organized into three layers with a sigmoid transfer function. Fig. 1 shows the topology of the FF network with the EBP. The initial weights, the biases, and the connection strengths between nodes were assigned as arbitrary small values. The weights and the biases gradually converged to optimum values during model training progresses that ensured the output values were close enough to the desired target outputs. The EBP training algorithm corrected the weights by minimizing the total error with the steepest descent. The stopping criteria for the modifying process are the sum of squared error and a maximum number of epochs, which implies that the error was minimal and the weights were optimal (Riad et al., 2004).

2.2 Flash Flood Routing Model (FFRM)

The FFRM is based on the dynamic wave theory using the Saint-Venant equations as followed

$$\frac{\partial A}{\partial t}+\frac{\partial Q}{\partial x}-q_1+q_2=0 \tag{1}$$

$$\frac{\partial Q}{\partial t}+\frac{\partial}{\partial x}\left(\frac{Q^2}{A}\right)+gA\left(\frac{\partial H}{\partial x}+S_f\right)-q_1V_1+q_2\left(\frac{Q}{A}\right)=0 \tag{2}$$

where A is the cross-sectional area [m^2], H is the stage [m], Q is the discharge [m^3/s], q_1 is the lateral inflow per unit channel length [$m^3/s/m$], q_2 is the lateral outflow per unit channel length [$m^3/s/m$], S_f is the friction slope [-], V_1 is the longitudinal velocity component of lateral inflow [m/s], g is the gravitational acceleration [m/s^2], t is the time [s], and x is the longitudinal distance along the channel [m]. The cross-sectional area is a function of water depth such that only two flow variables, Q and H,

Please cite as: *Hsu MH, Lin SH, Fu JC, Chung SF, Chen AS. (2010) Longitudinal stage profiles forecasting in rivers for flash floods, Journal of Hydrology, 388 (3-4), 426-437, DOI:10.1016/j.jhydrol.2010.05.028.*
to be solved for above equations.

Eqs. (1) and (2) are hyperbolic partial differential equations with two independent variables *Q* and *H*. A numerical solution can be obtained when the initial and the boundary conditions are appropriately prescribed. In this study, the upstream boundation conditions were from ANN, and the tidal stage was used as the downstream boundary condition. The four-point implicit finite-difference approximation (Amein and Fang, 1970) is employed to solve Eqs. (1) and (2). During the discretization process, the two adjoining cross-sections can be represented in two equations with four unknowns for flow variables at future time

$$\begin{aligned} C_\ell\left(Q_{\ell+1}^{t+1},H_{\ell+1}^{t+1},Q_\ell^{t+1},H_\ell^{t+1},Q_{\ell+1}^{t},H_{\ell+1}^{t},Q_\ell^{t},H_\ell^{t}\right)=0 \\ M_\ell\left(Q_{\ell+1}^{t+1},H_{\ell+1}^{t+1},Q_\ell^{t+1},H_\ell^{t+1},Q_{\ell+1}^{t},H_{\ell+1}^{t},Q_\ell^{t},H_\ell^{t}\right)=0 \end{aligned} \tag{3}$$

where C_ℓ and M_ℓ represent the discretized continuity and momentum equations between the ℓ^{th} and the $(\ell+1)^{\text{th}}$ cross-sections, respectively. *t* and (*t*+1) indicate the flow variables at the present-time and advanced-time, respectively. With *N* cross-sections, a total of (2*N*-2) equations with 2*N* unknowns should be yielded. The deficiencies are supplemented by boundary conditions to solve the unknown variables. The boundary conditions include the river stages at the most upstream cross sections or the discharges from upstream watersheds, and the tide stages at the downstream river mouth. Eq. (3) is solved by the Newton-Raphson iterative procedure.

In the process of data assimilation, the real time river stage observations from specific gauge stations are treated as the initial internal boundary conditions in the FFRM. Therefore, Eq. (3) is expanded by adding *K* equations for river stages at gauge stations, where *K* represents the total number of specfic gauge stations. The total number (2*N*+*K*) of equations is more than the unknowns of flow variables (2*N*). The equation

set becomes an over-determined system, which is solved by the least-squares method to find the optimum solution (Hsu et al., 2003). In the iterative procedure for solving the flow variables, the current increment of flow variables are expressed as

$$\Delta = \left[\mathrm{E}^T \mathrm{E} \right]^{-1} \cdot \left[\mathrm{E}^T R \right] \tag{4}$$

where, E is the extended matrix coefficient, R represents the residual (Hsu et al., 2003). In the FFRM, the real-time observed water stages are real values that may be different from the computed stages at the present-time. Hence, the model have to recalculate the flow variables at present time (t) from the previous time (t-1) by using the real-time observed water stages as the initial interior boundary conditions rather than the iterative computed stages at previous time (t-1) to improve the stage profiles forecasting. Fig. 2 illustrates the flood routing procedure. The results from the least-squares method of dynamic routing provide more accurate initiation for stage forecasting.

2.3 FFRM with interior boundaries from stage predictions of ANN (FFRM-ANN)

The above-mentioned FFRM provides a better initiation for data assimilaion. But the improvement gradually diminished when forecasting far ahead in time due to lack of the predicted stages at gauge stations (Hsu et al. 2003, 2006). The ANN algorithms are capable to solve problems by applying information acquired from experience to new problems and case scenarios (Haykin, 1999). We developed the flash flood routing model with the interior boundaries from stage predictions of ANN (FFRM-ANN) that integrates stages prediction with ANN at gauge stations and flash flood routing model for river stage profiles forecasting.

The FFRM-ANN predicted future river stages at gauge locations by ANN model based on current rainfalls and river stages, i.e., the rainfall forecasting over the lead-time was not considered. The stage predictions from ANN were regarded as the real stages at the advance time for adjusting model variables. The flood routing recalculated the flow variables at advance time (t+1) from the flow of present-time (t) to fit the internal boundary condition during the recalculation procedure. The least-squares method was used again to find the optimum forecasting of stage profiles. The routing proceeded with step by step to the advance time (t+2) and (t+3) in the similar way. The FFRM-ANN integrated the FFRM and the ANN algorithm to improve the accuracy of stage profile forecastings, which included the flood stages not only at the gauge stations but also for the unmeasured sites of the river.

3. Description of Study Site

The Tanshui River basin (Fig. 4), located in northern Taiwan, consists of three major tributaries: the Dahan River, the Sindian River and the Keelung River. The Metropolitan Taipei, with approximate 6 million populations, situates at the downstream floodplain of the Tanshui River. The main river channel is 328 km long with a catchment area 2,726 km^2 and the basin-averaged annual precipitation is 3,001 mm. The short river length and the steep bed slope, ranging from 0.15% to 27%, result in short concentration time from the upstream watersheds to the downstream floodplains as quick as 3 to 6 hours.

The damage caused by flooding in Taiwan is US $500 million/year (Yen et al., 1998). Inundations in the Metropolitan Taipei frequently occur and generate heavy losses when typhoons or severe rainstorms strike. The Taipei Flood Mitigation Project was initiated in 1982 to build a flood defense system to protect the Metropolitan

Taipei to against flooding up to 200-year return period. The major components in the project were engineering structures, including levees, a flood diversion channel (the Erchong Floodway, Fig. 4), pumping stations, flood control gates, drainage systems, and channel improvement. In addition to the hardware constructions, the Water Resources Agency (WRA) of the Ministry of Economic Affairs (MOEA) established the Tanshui River Flood Forecasting System to mitigate flood damage in 1977. An enhanced system that consisted of rainfall forecasting and rainfall-runoff forecasting models was developed for real-time river stage forecasting in December 1998 (Yen et al., 1998).

In this study, the computational transects of the FFRM were established by the surveyed cross-sectional profiles with 0.5 km intervals along the river. Fig. 4 presents the locations of the 235 computational transects. The upstream boundaries were Hsinhai Bridge for the Dahan River, Xiulang Bridge for the Sindian River, Bao Bridge for the Jingmei River (a tributary of the Sindian River), and Jieshou Bridge for the Keelung River. The downstream boundary was the river mouth. Fifteen river gauges that measure the river stages and transmit the observations hourly exist in the system. The measured river stages were applied to correct the current calculated flow conditions in the numerical model.

4. Training of ANN

We calibrated and verified the model parameters with the field data collected by the WRA. The root mean square error (RMSE) of differences between observed and computed stages was utilized for evaluating the model performance.

$$RMSE = \{\frac{1}{n}[\sum_{1}^{n}(H_c - H_o)^2]\}^{1/2} \quad (5)$$

where H_c is the computed water stage [m], H_0 is the observed water stage [m], and n is the total number of observed water stage [-].

4.1 Input Data and Structure of the Model

Based on the hourly rainfalls (P) and the river stages (H), this study predicted future river statges at gague locations by an ANN-based algorithm. The input vector includes rainfalls and river stages at the present time and previous three hours (i.e., *t*, *t*-1, *t*-2 and *t*-3). The output vector represents the river stage predictions for 1-3 hour lead time (i.e., *t*+1, *t*+2 and *t*+3). The small catchment area of the case study results in short concentration time from upstream watersheds to downstream floodplain such that only the rainfalls and the river stages within previous three hours were used to construct the ANN model. The ANN algorithm can be represented by the following compact form:

$$\mathbf{H} = ANN\left(\mathbf{X}\right) \tag{6}$$

Where $\mathbf{H} = \left(H^{t+1}, H^{t+2}, H^{t+3}\right)^T$ is the output vector of stage predictions at time t+1, t+2 and t+3; $\mathbf{X}$ is the input vector with elements $X_j^{t-k} \in \{P, H\}$, $j = 1, \ldots, s; k = 0, \ldots, (r-1)$, which represents the rainfall or stage of the predicting station and its upstream station j at time t-k, r is the input time dimension (r = 4 used in this study), s is the total number of the upstream rainfall and gauge stations. Eq. (6) indicates that the predicted river stages depend on the rainfalls and river stages of the predicting sites and its upstream stations of previous three hours and current time.

A trial-and-error procedure was applied to determine the optimum structure, including the dimention of input vector and the number of hidden nodes, of each

station for the ANN model.

4.2 ANN calibration and verification

Eight typhoon events that hit Taiwan between 2004 and 2005, accounting for 270 hours of rainfall and river stage pairs, were selected for model training. Five of these events that included the highest and the lowest of maximun rainfall intensities were used to calibrate the ANN model (Table 1). Fig. 3 shows the locations of the Tahshui River Basin with 19 rainfall and 15 stage gauges. We analyzed the correlation and determined the lag time between the rainfall at rain gauge stations and the river stages at hydrologic gauge stations. Taking gauge station B1 as an example, the rain gauge stations R1, R2, and R3 are located in the upstream of B1, therefore the initial setting of input vector included the hydologic informations at R1, R2, R3 and B1 between present time and three hours before, which was expressed as a vector with 16 components [$(R1)^{t-3}$, $(R1)^{t-2}$, $(R1)^{t-1}$, $(R1)^{t}$, $(R2)^{t-3}$, $(R2)^{t-2}$, $(R2)^{t-1}$, $(R2)^{t}$, $(R3)^{t-3}$, $(R3)^{t-2}$, $(R3)^{t-1}$, $(R3)^{t}$, $(B1)^{t-3}$, $(B1)^{t-2}$, $(B1)^{t-1}$, $(B1)^{t}$]. A trial-and-error procedure was applied to determine the optimum structure, including the dimention of input vector and the number of hidden nodes, for each station in the ANN model. The optimized structures of ANN model for all stations are listed in Table 2. The dimension of input vector, the number of hidden nodes, and the dimension of ouput vector for B1 station were 11, 5, and 3, respectively. Out of the 16 components, 11 were selected as the input vector and 5 were considered as hidden nodes. The outputs were the stage forecasting in next three hours, which can be shown as [$(B1)^{t+1}$, $(B1)^{t+2}$, $(B1)^{t+3}$]. Table 3 lists the calibration results of the ANN at the boundary and the interior stations of the FFRM. The interior boundary stations, which the input dimension included the the rainfall and the observed upstream stages, had better performance

than the boundary ones, which used the rainfall only. We further applied the calibrated model to three typhoon events for model verification. Table 4 lists the verification results that the model performed constitenly for the interior stations, but the accuracy dropped for the boundary stations. The predictions for the Bao Bridge were the worst among all stations due to the small upstream catchment area, which resulted in short concentration time that was less than one hour.

5. Model Application and Analysis

The Manning's roughness coefficient was an important parameter that significantly affected the computed river stages in the FFRM. A traditional trial-and-error method was used to calibrate the coefficient using the field data of four historical events of the Tanshui River basin collected by the WRA in four typhoon events. Table 5 lists the calibrated Manning's roughness values for the segments of the Tanshui River System.

The FFRM and ANN models were coupled to forecast the river stages of three typhoons, i.e., Aere (2004), Haima (2004) and Haitang (2005). Since the Tanshui River is a tidal river, the present-time observed tide stage at the river mouth can be taken as the downstream boundary condition. In addition, the summation of the astronomical tide and the meteorological tide at the river mouth was specified as the 3 hours leading downstream boundary condition (Hsu et al., 2000). For the FFRM, the boundary conditions were the observed river stages. For the FFRM-ANN, the boundary conditions included the current river stages obtained from real-time observations and the advance river stages predicted by the ANN algorithm. The difference between the results of the FFRM and the FFRM-ANN were also compared.

Fig. 5 plots the river stage forecasting and observed hydrographs of Typhoon Aere at Chungcheng Bridge, Taipei Bridge and Dazhi Bridge. Despite the good fitness for the predictions at the Chungcheng Bridge, the FFRM over-estimated the stages at the Taipei Bridge and under-estimated the stages at the Dazhi Bridge. The RMSEs were more than 1 m for the 3-hr forecasting for the two sites. With the improved interior boundary condition using the ANN, the FFRM-ANN predictions were much closer to the observed data. Fig. 5 shows the modeling results for Typhoon Haima event of the FFRM and the FFRM-ANN predictions at the same sites as in Fig. 5. Both models performed better than Typhoon Aere event at Taipei Bridge, obviously, due to the tidal cycle dominated the stage variation at Taipei Bridge during the event. The FFRM predictions at Dazhi Bridge remained poor with more than five times of RMSE as that of the FFRM-ANN, as shown in Fig. 6-(c). Fig. 7 illustrates the predictions of the FFRM and the FFRM-ANN at the same sites as in Fig. 5 for Typhoon Haitang event. Again, the FFRM-ANN had consistent performance for all sites and the FFRM model failed to forecast the stages at Taipei Bridge and Dazhi Bridge.

The results of the above three events also indicated that the FFRM-ANN predictions of peak stages and timings matched the observations with less than one hour of time lag. The FFRM failed to capture these critical features of the events, which are crucial for decision makings to mitigate flood disasters.

Fig. 8 summarizes the RMSE for the forecast with various lead times of the three typhoon events at Dazhi Bridge. For the FFRM, the improvement with real-time stage correction method gradually diminished when the lead time increased. The greater RMSE values for 2-hr and 3-hr ahead of time predictions represented that the errors grew as the lead time went far. Besides, the RMSE for the FFRM-

ANN were close to the ANN model predictions at river gauge stations. Obviously, the RMSE of the flood routing by the FFRM-ANN were always lower than the predictions calculated by the FFRM. Fig. 9 compares the averaged RMSE of the three typhoon events for various lead times at Chungcheng Bridge, Taipei Bridge, and Dazhi Bridge. The RMSE apparently dropped in the FFRM-ANN with the ANN correction of interior boundary conditions, especially for Taipei Bridge and Dazhi Bridge.

Both the FFRM and the FFRM-ANN can provide the longitudinal stage profiles forecasting, not only at gauged sites but also for the un-gauged sites of a whole river system. Fig. 10 shows the observed and forecasted longitudinal spatial variations of river peak stage along the Tanshui River for Typhoon Aere. The predictions from both models at Shizitou and Rukou Weir were close to the observations. Nevertheless, the FFRM considerably over-predicted the peak stages at Tudigonbi and Taipei Bridge, The forecasting errors at Taipei Bridge were more than 1.5m in the FFRM. With the improved interior stage predictions from the ANN, the errors declined to less than 0.3m in the FFRM-ANN.

For Typhoon Haima event, shown as Fig. 11, the FFRM under-estimated the stages for the downstream segments and over-predicted for the upstream segments. The FFRM-ANN had similar behavior, however, the RMSE were only about 30% of the FFRM ones. The peak stage observation and prediction profiles for Typhoon Haitang event are compared in Fig. 12. The FFRM-ANN performed superior than the FFRM for all gauges. The enhanced predictions at river gauges in the FFRM-ANN provided more reliable profile forecasting along the rivers.

The accuracy of the river stage profiles can provide flood warning information

along the river other than gauge stations. For example, The Keelung River channel width suddenly reduces from about 350m to 100m at the Chungshan Bridge, where has no river gauge at this critical section, as shown in Fig. 3. The FFRM itself was not capable of forecasting, but the coupled FFRM-ANN successfully forecasted the river stages at locations in between gauge stations. Fig. 13 is the hourly predictions of stages with 1, 2 and 3-hr lead time from the FFRM-ANN at Chungshan Bridge for Typhoon Aere event. The information successfully helped the water authority to predict the flood conditions for emergency operations during typhoons.

6. Conclusions

The FFRM-ANN was developed and applied to the Tanshui River System for forecasting the longitudinal flood stage profiles. In the FFRM-ANN, the real-time stage observations and the ANN predictions at river gauge stations were used as the interior boundary conditions for data assimilation. The model parameters were calibrated and verified against field measurements of historical typhoon events. The agreement between the model predictions and the measurement demonstrated that the model had improved the accuracy of subsequent forecasting to provide reliable real-time warning information. The modeling results showed that FFRM-ANN performed better river stage forecasting at gauge stations than the FFRM, due to the interior boundary conditions imposed for the dynamic routing model.

Acknowledgments

The authors express their grateful appreciation to the National Science Council of Taiwan for the research funding (Grant No. NSC 97-2221-E-002-141-MY3) and the Water Resources Agency for providing the field data.

Please cite as: *Hsu MH, Lin SH, Fu JC, Chung SF, Chen AS. (2010) Longitudinal stage profiles forecasting in rivers for flash floods, Journal of Hydrology, 388 (3-4), 426-437, DOI:10.1016/j.jhydrol.2010.05.028.*

References

Amein, M., Fang, C.S., 1970. Implicit flood routing in natural channels. J. Hydraul. Divis., ASCE, 96 (5) 2481-2500.

Campolo, M., Andreussi, P., Soldati, A., 1999. River Flood Forecasting with a Neural Network Model. Water Resour. Res., 35 (4) 1191-1197.

Chang, F.J., Chang, L.C., Huang, H.L., 2002. Real-time recurrent learning neural network for stream-flow forecasting. Hydrolog. Process., 16 (13) 2577-2588.

Chiang, Y.M., Hsu, K.L., Chang, F.J., Hong, Y., Sorooshian, S., 2007. Merging multiple precipitation sources for flash flood forecasting. J. Hydrolog., 340 (3-4) 183-196.

Diamantopoulou, M.J., Georgiou, P.E., Papamichail, D.M., 2006. A time delay artificial neural network approach for flow routing in a river system. Hydrol. Earth Syst. Sci. Discuss., 3 2735-2756.

Ford, D.T., 2001. Flood-Warning Decision-Support System for Sacramento, California. J. Water Resour. Plan. Manag., 127 (4) 254-260.

Haykin, S.S., 1999. Neural networks. A Comprehensive Foundation. Prentice Hall, Upper Saddle River, N.J.

Hsu, M.H., Fu, J.C., Liu, W.C., 2003. Flood routing with real-time stage correction method for flash flood forecasting in the Tanshui River, Taiwan. J. Hydrolog., 283 (1-4) 267-280.

Hsu, M.H., Fu, J.C., Liu, W.C., 2006. Dynamic Routing Model with Real-Time Roughness Updating for Flood Forecasting. J. Hydraul. Eng., 132 (6) 605-619.

Hsu, M.H., Lin, S.H., Fu, J.C., 2000. Flood forecast system model for Tanshui River basin, (IV): flood routing model, Hydroinformatics 2000 Conference, University of Iowa, Iowa.

Littlewood, I.G., Clarke, R.T., Collischonn, W., Croke, B.F.W., 2007. Predicting daily streamflow using rainfall forecasts, a simple loss module and unit hydrographs: Two Brazilian catchments. Environmental Modelling & Software., 22 (9) 1229-1239.

Rajurkar, M.P., Kothyari, U.C., Chaube, U.C., 2004. Modeling of the daily rainfall-runoff relationship with artificial neural network. J. Hydrolog., 285 (1-4) 96-113.

Riad, S., Mania, J., Bouchaou, L., Najjar, Y., 2004. Predicting catchment flow in a semi-arid region via an artificial neural network technique. Hydrolog. Process., 18 (13) 2387-2393.

Saavedra, I., Lopez, J.L., Garcia-Martinez, R., 2003. Dynamic Wave Study of Flow in Tidal Channel System of San Juan River. J. Hydraul. Eng., 129 (7) 519-526.

Sabino, A.A., Querido, A.L., Sousa, M.I., 1999. Flood management in Cape Verde. The case study of Praia. Urban Water, 1 161-166.

Simon, H., 1999. Neural network: a comprehensive foundation. Second Edition. Prentice Hall.

Please cite as: *Hsu MH, Lin SH, Fu JC, Chung SF, Chen AS. (2010) Longitudinal stage profiles forecasting in rivers for flash floods, Journal of Hydrology, 388 (3-4), 426-437, DOI:10.1016/j.jhydrol.2010.05.028.*

Sudheer, K. P., Gosain, A. K., Ramasastri, K. S., 2002. A data-driven algorithm for constructing artificial neural network rainfall-runoff models. Hydrolog. Process., 16 (6) 1325-1330.

Yen, C.L., Lee, T.H., Wang, R.Y., Yang, D.L., Hsu, M.H., 1998. Research and development of flood forecasting system model for Tanshui River Basin, Technical Report. Water Resources Agency of the Ministry of Economic Affairs. (in Chinese).

Please cite as: *Hsu MH, Lin SH, Fu JC, Chung SF, Chen AS. (2010) Longitudinal stage profiles forecasting in rivers for flash floods, Journal of Hydrology, 388 (3-4), 426-437, DOI:10.1016/j.jhydrol.2010.05.028.*

Figure captions

Please cite as: *Hsu MH, Lin SH, Fu JC, Chung SF, Chen AS. (2010) Longitudinal stage profiles forecasting in rivers for flash floods, Journal of Hydrology, 388 (3-4), 426-437, DOI:10.1016/j.jhydrol.2010.05.028.*

Table 1. Typhoon events information for ANN model training

Training	Typhoon Event	Time of start (LTC)	Time of end (LTC)	Maximum rainfall intensity (mm/hr)	Number of hours
Calibration	Nockten	2004/10/24 9:00	2004/10/25 21:00	70.0	36
	Matsa	2005/08/04 10:00	2005/08/05 21:00	32.0	35
	Talim	2005/08/31 9:00	2005/09/01 10:00	59.0	25
	Khanun	2005/09/10 15:00	2005/09/11 05:00	36.0	14
	Longwang	2005/10/01 12:00	2005/10/02 13:00	53.0	25
Verification	Aere	2004/08/23 9:00	2004/08/25 11:00	53.0	50
	Haima	2004/09/11 02:00	2004/09/12 20:00	69.0	42
	Haitang	2005/07/17 02:00	2005/07/18 21:00	44.0	43
Total hourly values of rainfall and river stage pairs					270

Please cite as: *Hsu MH, Lin SH, Fu JC, Chung SF, Chen AS. (2010) Longitudinal stage profiles forecasting in rivers for flash floods, Journal of Hydrology, 388 (3-4), 426-437, DOI:10.1016/j.jhydrol.2010.05.028.*

Table 2. The input data of the ANN algorithm

Type	Output gauge station	Input gauge station and time dimension	Structure of ANN
Boundary station	$(B1)^{t+1}$, $(B1)^{t+2}$, $(B1)^{t+3}$ (B1:Hsinhai Bridge)	$(R1)^{t-2}$, $(R1)^{t-1}$, $(R1)^{t}$, $(R2)^{t-2}$, $(R2)^{t-1}$, $(R2)^{t}$, $(R3)^{t-2}$, $(R3)^{t-1}$, $(R3)^{t}$, $(B1)^{t-1}$, $(B1)^{t}$,	11-5-3
	$(B2)^{t+1}$, $(B2)^{t+2}$, $(B2)^{t+3}$ (B2:Xiulang Bridge)	$(R7)^{t-2}$, $(R7)^{t-1}$, $(R7)^{t}$, $(R8)^{t-2}$, $(R8)^{t-1}$, $(R8)^{t}$, $(R9)^{t-2}$, $(R9)^{t-1}$, $(R9)^{t}$, $(R10)^{t-1}$, $(R10)^{t}$, $(B2)^{t-1}$, $(B2)^{t}$,	13-6-3
	$(B3)^{t+1}$, $(B3)^{t+2}$, $(B3)^{t+3}$ (B3:Bao Bridge)	$(R4)^{t-2}$, $(R4)^{t-1}$, $(R4)^{t}$, $(R5)^{t-2}$, $(R5)^{t-1}$, $(R5)^{t}$, $(R6)^{t-2}$, $(R6)^{t-1}$, $(R6)^{t}$, $(B3)^{t-1}$, $(B3)^{t}$,	11-7-3
	$(B4)^{t+1}$, $(B4)^{t+2}$, $(B4)^{t+3}$ (B4:Jieshou Bridge)	$(R11)^{t-2}$, $(R11)^{t-1}$, $(R11)^{t}$, $(R12)^{t-2}$, $(R12)^{t-1}$, $(R12)^{t}$, $(B4)^{t-1}$, $(B4)^{t}$,	8-7-3
Interior station	$(H1)^{t+1}$, $(H1)^{t+2}$, $(H1)^{t+3}$ (H1:Chungcheng Bridge)	$(R13)^{t}$, $(R14)^{t}$, $(H1)^{t-1}$, $(H1)^{t}$, $(B2)^{t-1}$, $(B2)^{t}$, $(B3)^{t-1}$, $(B3)^{t}$,	8-5-3
	$(H2)^{t+1}$, $(H2)^{t+2}$, $(H2)^{t+3}$ (H2:Rukou Weir)	$(R13)^{t}$, $(R14)^{t-1}$, $(R14)^{t}$, $(B1)^{t-1}$, $(B1)^{t}$, $(H1)^{t-1}$, $(H1)^{t}$, $(H2)^{t-1}$, $(H2)^{t}$,	9-8-3
	$(H3)^{t+1}$, $(H3)^{t+2}$, $(H3)^{t+3}$ (H3:Taipei Bridge)	$(R14)^{t-1}$, $(R14)^{t}$, $(R15)^{t-1}$, $(R15)^{t}$, $(B1)^{t-1}$, $(B1)^{t}$, $(H1)^{t-1}$, $(H1)^{t}$, $(H2)^{t-1}$, $(H2)^{t}$, $(H3)^{t-1}$, $(H3)^{t}$,	12-8-3
	$(H4)^{t+1}$, $(H4)^{t+2}$, $(H4)^{t+3}$ (H4:Shizitou)	$(R14)^{t-2}$, $(R14)^{t-1}$, $(R14)^{t}$, $(R15)^{t-2}$, $(R15)^{t-1}$, $(R15)^{t}$, $(B1)^{t-2}$, $(B1)^{t-1}$, $(B1)^{t}$, $(H1)^{t-2}$, $(H1)^{t-1}$, $(H1)^{t}$, $(H2)^{t-1}$, $(H2)^{t}$, $(H3)^{t-1}$, $(H3)^{t}$, $(H4)^{t-1}$, $(H4)^{t}$,	18-12-3
	$(H5)^{t+1}$, $(H5)^{t+2}$, $(H5)^{t+3}$ (H5:Tudigonbi)	$(R14)^{t-2}$, $(R14)^{t-1}$, $(R14)^{t}$, $(R15)^{t-2}$, $(R15)^{t-1}$, $(R15)^{t}$, $(R16)^{t}$, $(R17)^{t}$, $(B1)^{t-2}$, $(B1)^{t-1}$, $(B1)^{t}$, $(H1)^{t-2}$, $(H1)^{t-1}$, $(H1)^{t}$, $(H2)^{t-1}$, $(H2)^{t}$, $(H3)^{t-1}$, $(H3)^{t}$, $(H4)^{t-1}$, $(H4)^{t}$, $(H5)^{t-1}$, $(H5)^{t}$,	22-18-3
	$(H6)^{t+1}$, $(H6)^{t+2}$, $(H6)^{t+3}$ (H6:Wudu)	$(R11)^{t-2}$, $(R11)^{t-1}$, $(R11)^{t}$, $(R12)^{t-1}$, $(R12)^{t}$, $(R18)^{t}$, $(B4)^{t-1}$, $(B4)^{t}$, $(H6)^{t-1}$, $(H6)^{t}$,	10-8-3
	$(H7)^{t+1}$, $(H7)^{t+2}$, $(H7)^{t+3}$ (H7:Zhang-an Bridge)	$(R11)^{t-2}$, $(R11)^{t-1}$, $(R11)^{t}$, $(R12)^{t-1}$, $(R12)^{t}$, $(R18)^{t}$, $(B4)^{t-1}$, $(B4)^{t}$, $(H6)^{t}$, $(H7)^{t-1}$, $(H7)^{t}$,	11-11-3
	$(H8)^{t+1}$, $(H8)^{t+2}$, $(H8)^{t+3}$ (H8:Shehou Bridge)	$(R11)^{t-2}$, $(R11)^{t-1}$, $(R11)^{t}$, $(R12)^{t-1}$, $(R12)^{t}$, $(R18)^{t}$, $(R19)^{t}$, $(B4)^{t-1}$, $(B4)^{t}$, $(H6)^{t}$, $(H7)^{t}$, $(H8)^{t-1}$, $(H8)^{t}$,	13-10-3
	$(H9)^{t+1}$, $(H9)^{t+2}$, $(H9)^{t+3}$ (H9:Da-zhi Bridge)	$(R11)^{t-3}$, $(R11)^{t-2}$, $(R11)^{t-1}$, $(R11)^{t}$, $(R12)^{t-2}$, $(R12)^{t-1}$, $(R12)^{t}$, $(R18)^{t-1}$, $(R18)^{t}$, $(R19)^{t}$, $(B4)^{t-1}$, $(B4)^{t}$, $(H6)^{t-1}$, $(H6)^{t}$, $(H7)^{t}$, $(H8)^{t}$, $(H9)^{t-1}$, $(H9)^{t}$,	18-14-3
	$(H10)^{t+1}$,$(H10)^{t+2}$,$(H10)^{t+3}$ (H10:Bailing Bridge)	$(R11)^{t-3}$, $(R11)^{t-2}$, $(R11)^{t-1}$, $(R11)^{t}$, $(R12)^{t-2}$, $(R12)^{t-1}$, $(R12)^{t}$, $(R18)^{t-1}$, $(R18)^{t}$, $(R19)^{t-1}$, $(R19)^{t}$, $(B4)^{t-1}$, $(B4)^{t}$, $(H6)^{t-1}$, $(H6)^{t}$, $(H7)^{t-1}$, $(H7)^{t}$, $(H8)^{t-1}$, $(H8)^{t}$, $(H9)^{t}$, $(H10)^{t-1}$, $(H10)^{t}$,	22-16-3

R5 — Rainfall of rain-gauge station 5; H6 — River stage of hydrologic gauge station number 6;

B3 — River stage of boundary number 3;

superscript-(t) — real-time; superscript-(t-1) — previous one hour, and so on.

11-5-3 — means the dimension of input vector - the number of hidden nodes- the dimension of output vector.

Please cite as: *Hsu MH, Lin SH, Fu JC, Chung SF, Chen AS. (2010) Longitudinal stage profiles forecasting in rivers for flash floods, Journal of Hydrology, 388 (3-4), 426-437, DOI:10.1016/j.jhydrol.2010.05.028.*

Table 3. Statistical accuracy measures of ANN (calibration)

Type	Station	RMSE (m)		
		1-hr forecast	2-hr forecast	3-hr forecast
Boundary station of the FFRM	Hsinhai Bridge	0.173	0.274	0.411
	Xiulang Bridge	0.106	0.143	0.212
	Bao Bridge	0.156	0.223	0.375
	Jieshou Bridge	0.133	0.188	0.262
Mean		0.142	0.207	0.315
Interior station of the FFRM	Chungcheng Bridge	0.106	0.192	0.251
	Rukou Weir	0.087	0.150	0.215
	Taipei Bridge	0.110	0.176	0.223
	Shizitou	0.068	0.094	0.125
	Tudigonbi	0.092	0.115	0.120
	Wudu	0.138	0.214	0.367
	Zhangan Bridge	0.098	0.150	0.253
	Shehou Bridge	0.159	0.220	0.310
	Dazhi Bridge	0.115	0.174	0.211
	Bailing Bridge	0.095	0.122	0.142
Mean		0.107	0.161	0.222

Please cite as: *Hsu MH, Lin SH, Fu JC, Chung SF, Chen AS. (2010) Longitudinal stage profiles forecasting in rivers for flash floods, Journal of Hydrology, 388 (3-4), 426-437, DOI:10.1016/j.jhydrol.2010.05.028.*

Table 4. Statistical accuracy measures of ANN (verification)

Type	Station	RMSE (m)		
		1-hr forecast	2-hr forecast	3-hr forecast
Boundary station of the FFRM	Hsinhai Bridge	0.231	0.313	0.447
	Xiulang Bridge	0.227	0.318	0.459
	Bao Bridge	0.380	0.722	0.975
	Jieshou Bridge	0.200	0.316	0.422
Mean		0.259	0.417	0.576
Interior station of the FFRM	Chungcheng Bridge	0.094	0.160	0.208
	Rukou Weir	0.087	0.162	0.225
	Taipei Bridge	0.088	0.143	0.183
	Shizitou	0.068	0.086	0.113
	Tudigonbi	0.075	0.087	0.094
	Wudu	0.157	0.261	0.437
	Zhangan Bridge	0.108	0.190	0.334
	Shehou Bridge	0.175	0.243	0.361
	Dazhi Bridge	0.113	0.164	0.194
	Bailing Bridge	0.092	0.106	0.120
Mean		0.106	0.160	0.227

Please cite as: *Hsu MH, Lin SH, Fu JC, Chung SF, Chen AS. (2010) Longitudinal stage profiles forecasting in rivers for flash floods, Journal of Hydrology, 388 (3-4), 426-437, DOI:10.1016/j.jhydrol.2010.05.028.*

Table 5. Roughness values calibrated by the four typhoon events

River segment	Manning's roughness coefficient	River segment	Manning's roughness coefficient
Hsinhai Bridge – Rukou weir	0.033	Jieshou Bridge – Wudu	0.045
Xiulang – Chungcheng Bridge	0.033	Wudu – Zhangan Bridge	0.045
Bao – Chungcheng Bridge	0.035	Zhangan – Shehou Bridge	0.040
Chungcheng Bridge – Rukou weir	0.019	Shehou – Dazhi Bridge	0.035
Erchong Floodway	0.033	Dazhi – Bailing Bridge	0.035
Rukou weir – Taipei Bridge	0.030	Bailing Bridge – Shizitou	0.025
Taipei Bridge – Shizitou	0.029	Shizitou – river mouth	0.025

Please cite as: *Hsu MH, Lin SH, Fu JC, Chung SF, Chen AS. (2010) Longitudinal stage profiles forecasting in rivers for flash floods, Journal of Hydrology, 388 (3-4), 426-437, DOI:10.1016/j.jhydrol.2010.05.028.*

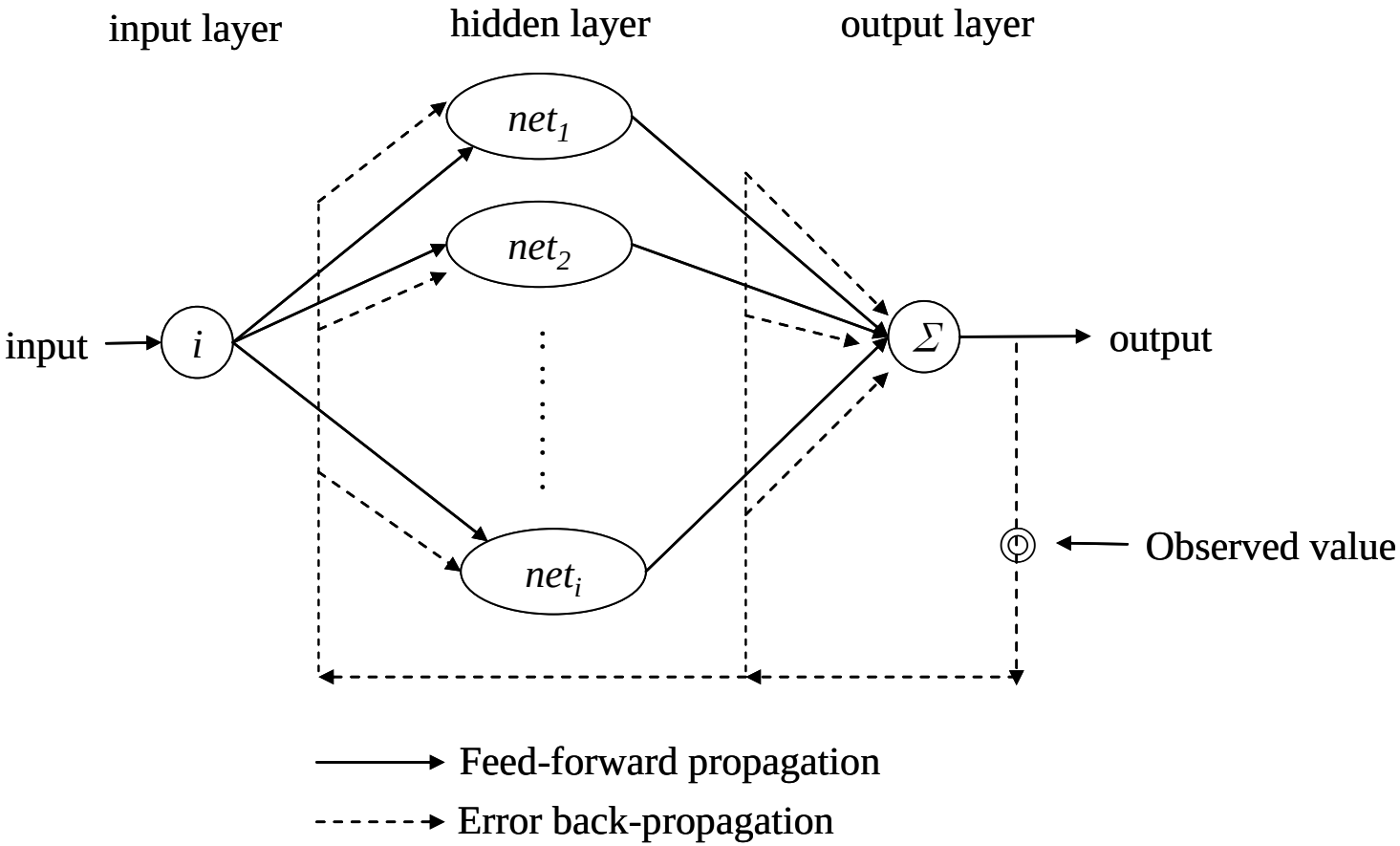

Figure 1. Topology of the feed-forward neural network with the error back-propagation.

Please cite as: *Hsu MH, Lin SH, Fu JC, Chung SF, Chen AS. (2010) Longitudinal stage profiles forecasting in rivers for flash floods, Journal of Hydrology, 388 (3-4), 426-437, DOI:10.1016/j.jhydrol.2010.05.028.*

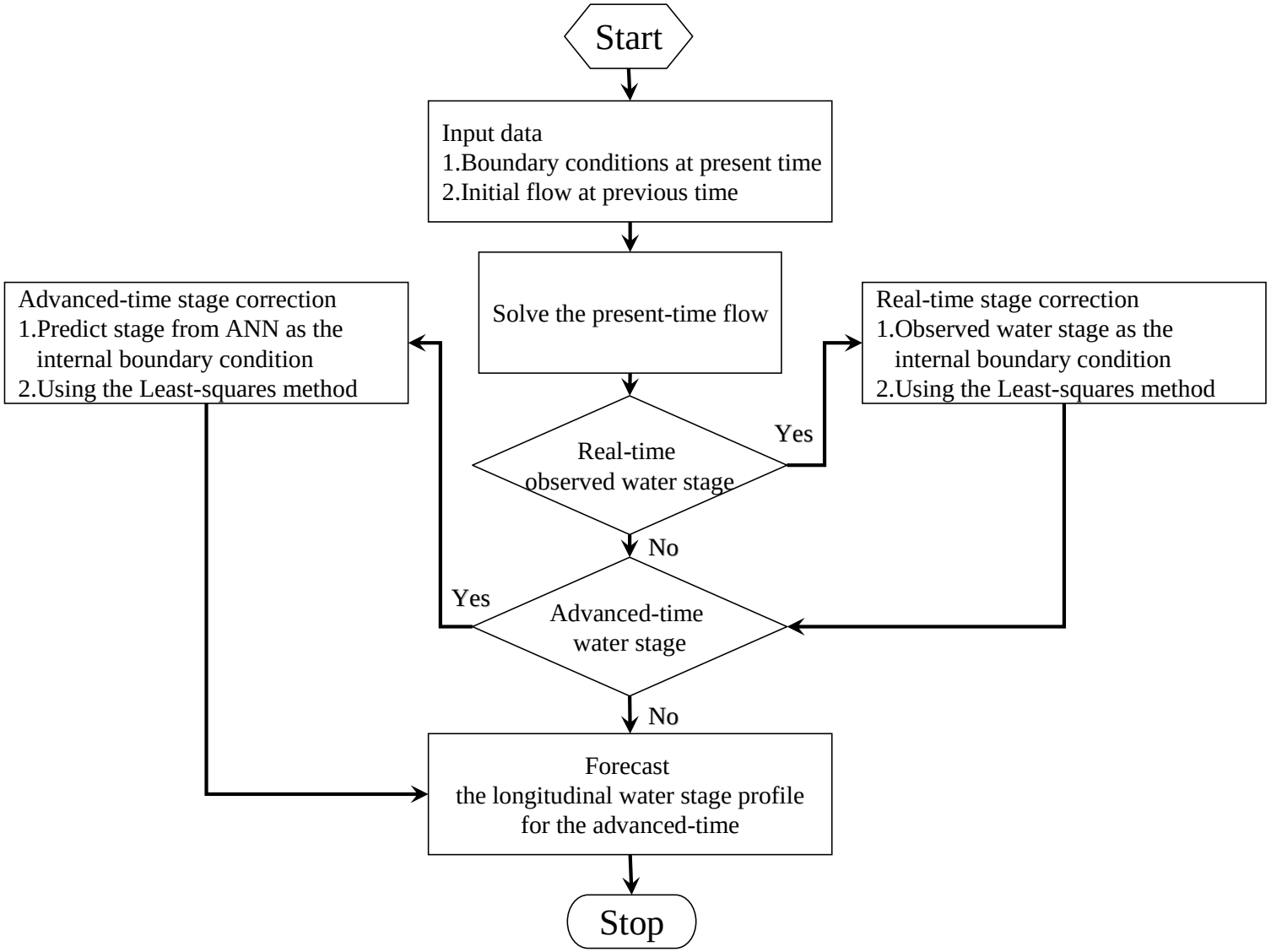

Figure 2. The procedures for flood routing and forecasting calculations.

Please cite as: *Hsu MH, Lin SH, Fu JC, Chung SF, Chen AS. (2010) Longitudinal stage profiles forecasting in rivers for flash floods, Journal of Hydrology, 388 (3-4), 426-437, DOI:10.1016/j.jhydrol.2010.05.028.*

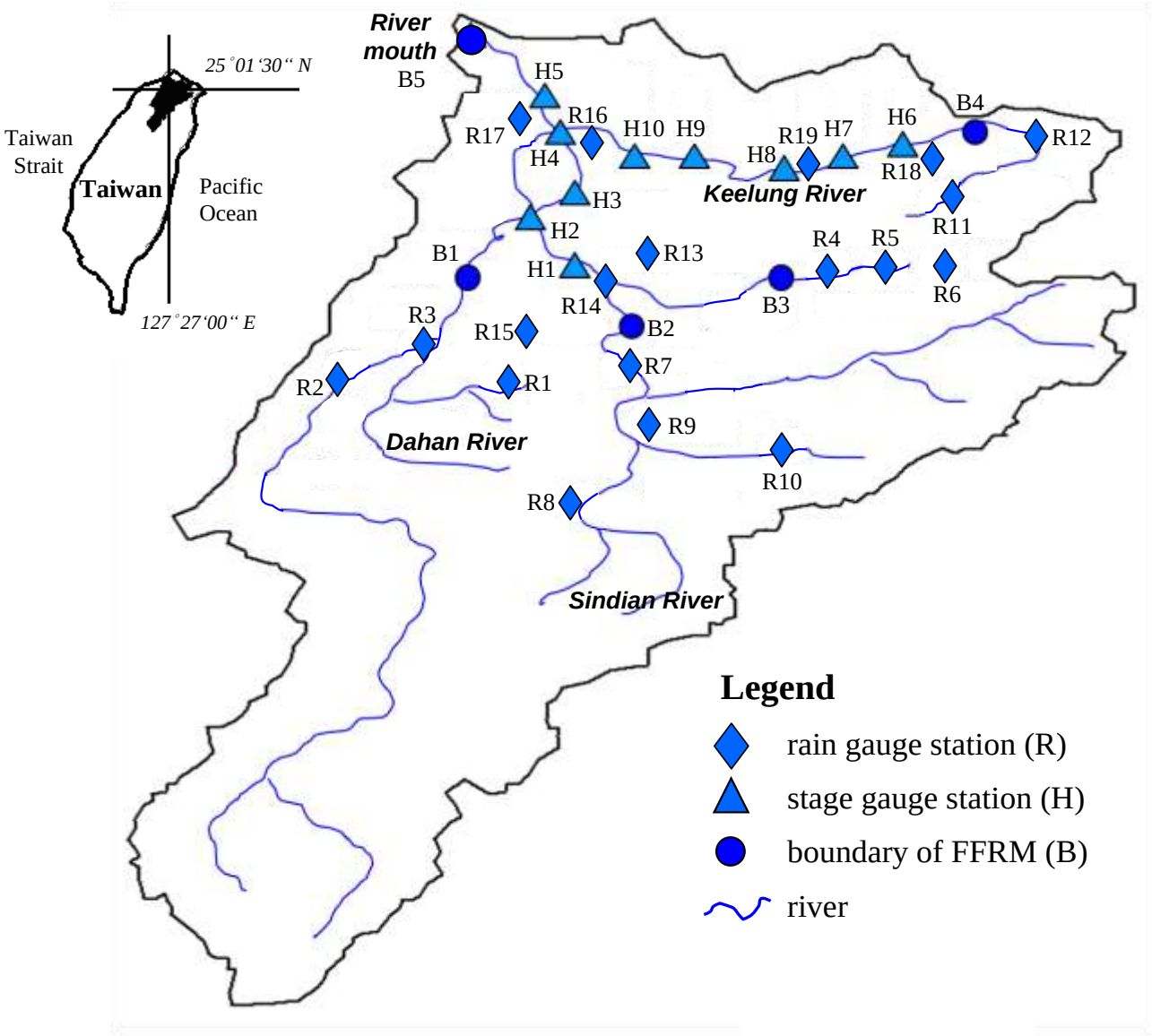

Figure 3. Locations of rain gauges, stage gauges and boundary stations of the Tanshui River system.

Please cite as: *Hsu MH, Lin SH, Fu JC, Chung SF, Chen AS. (2010) Longitudinal stage profiles forecasting in rivers for flash floods, Journal of Hydrology, 388 (3-4), 426-437, DOI:10.1016/j.jhydrol.2010.05.028.*

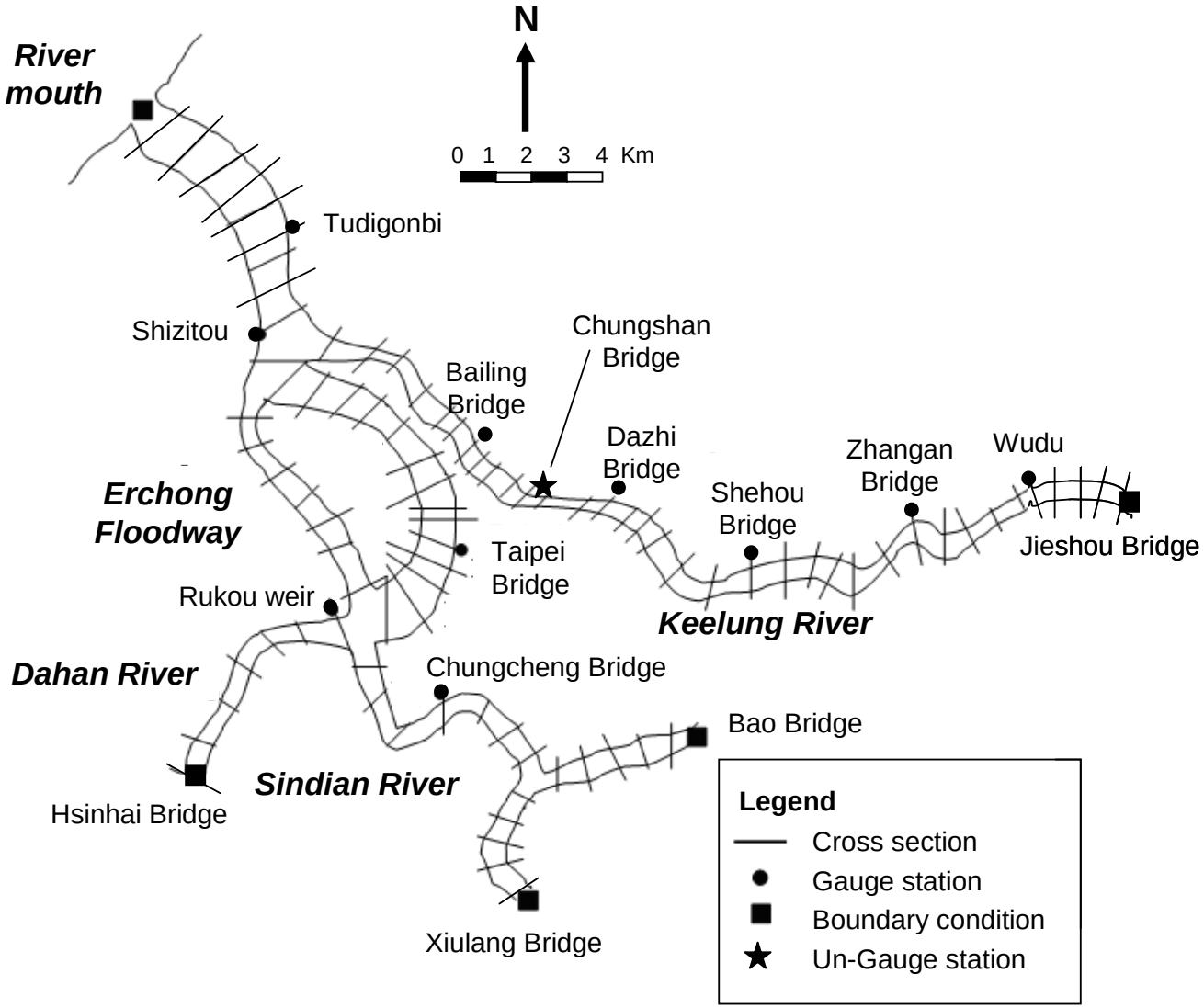

Figure 4. Layout of the Tanshui River system.

Please cite as: *Hsu MH, Lin SH, Fu JC, Chung SF, Chen AS. (2010) Longitudinal stage profiles forecasting in rivers for flash floods, Journal of Hydrology, 388 (3-4), 426-437, DOI:10.1016/j.jhydrol.2010.05.028.*

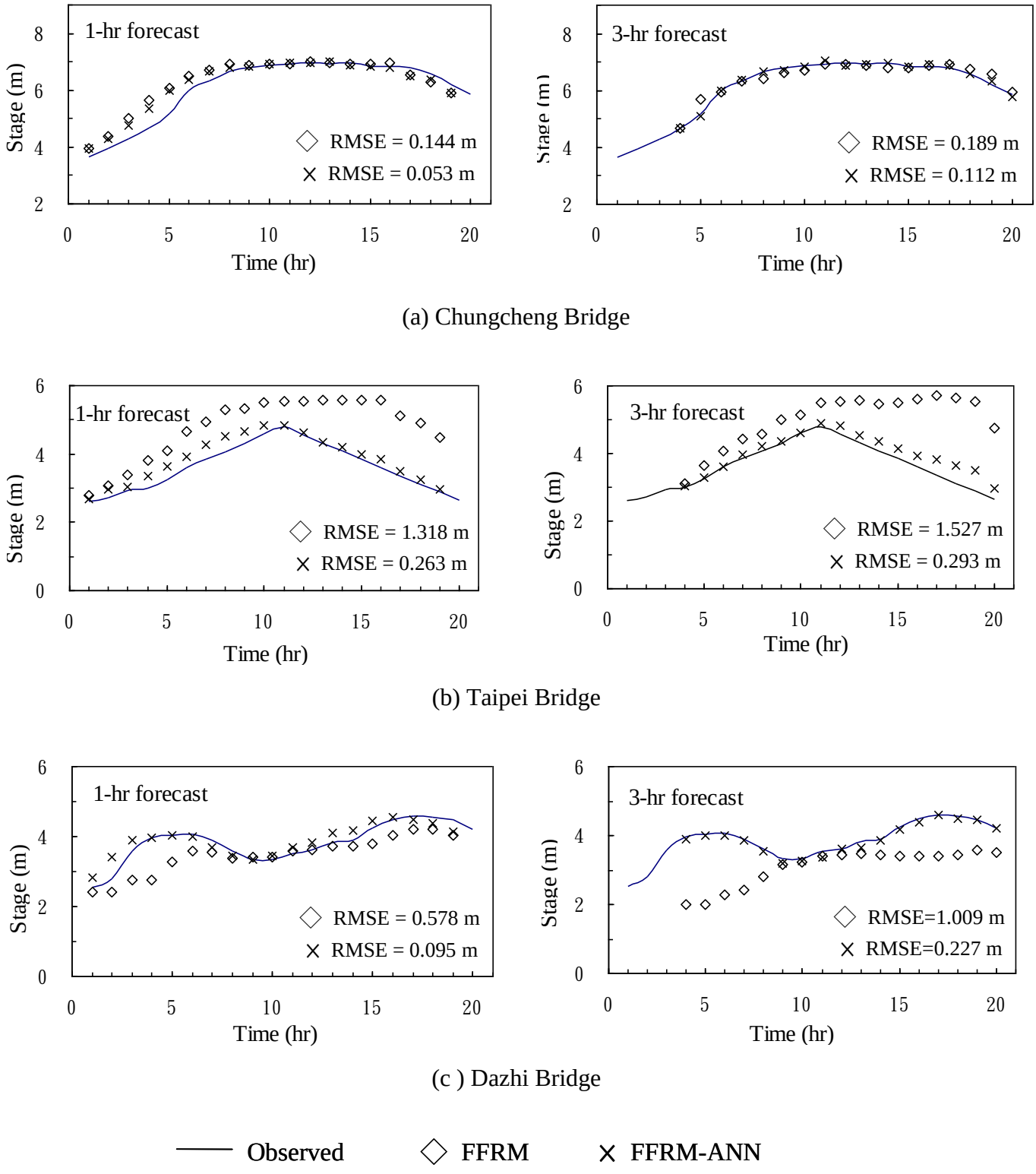

Figure 5. The forecasted river stage hydrographs at the Chungcheng, Taipei, and Dazhi Bridge for Typhoon Aere event.

Please cite as: *Hsu MH, Lin SH, Fu JC, Chung SF, Chen AS. (2010) Longitudinal stage profiles forecasting in rivers for flash floods, Journal of Hydrology, 388 (3-4), 426-437, DOI:10.1016/j.jhydrol.2010.05.028.*

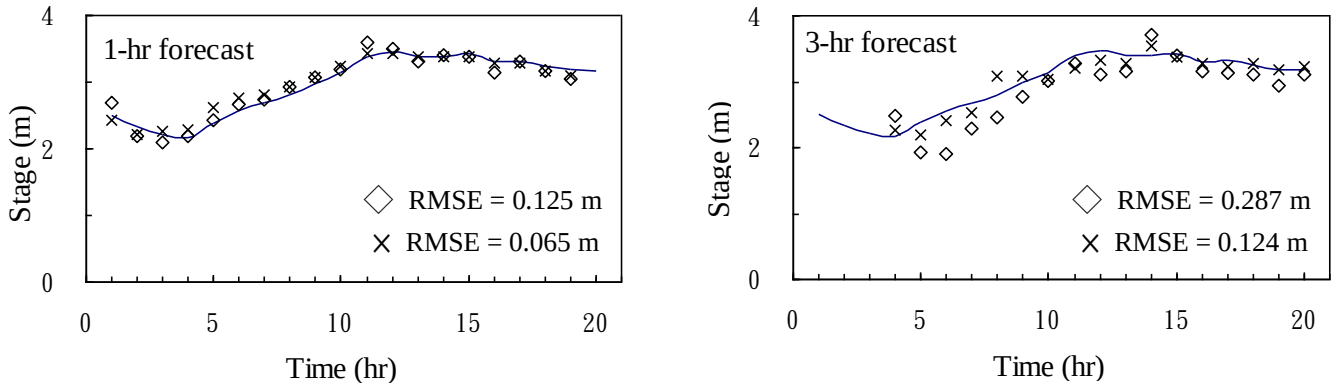

(a) Chungcheng Bridge

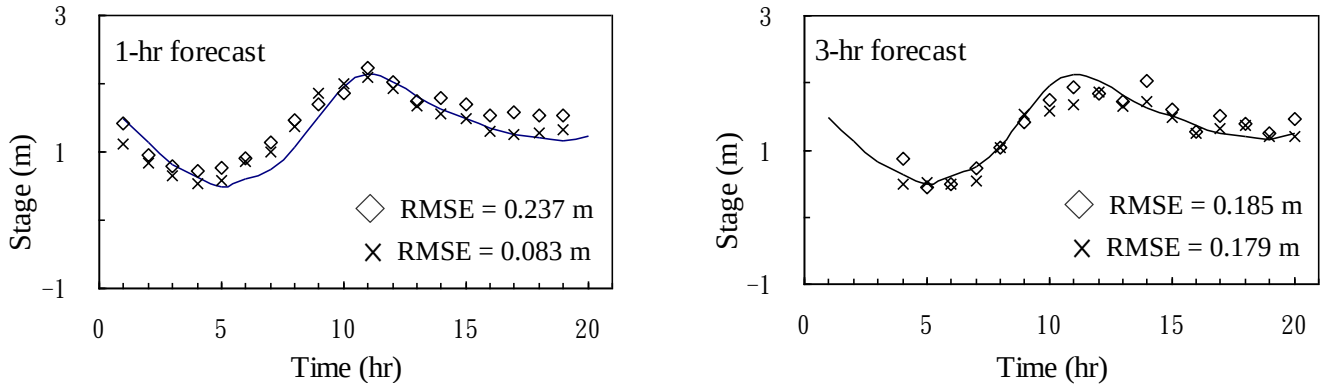

(b) Taipei Bridge

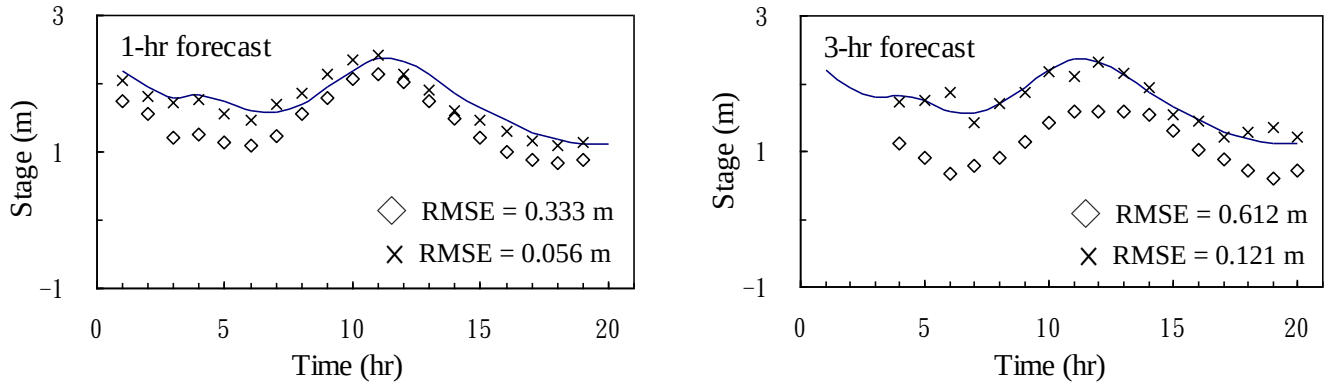

(c) Dazhi Bridge

Figure 6. The forecasted river stage hydrographs at the Chungcheng, Taipei, and Dazhi Bridge for Typhoon Haima event.

Please cite as: *Hsu MH, Lin SH, Fu JC, Chung SF, Chen AS. (2010) Longitudinal stage profiles forecasting in rivers for flash floods, Journal of Hydrology, 388 (3-4), 426-437, DOI:10.1016/j.jhydrol.2010.05.028.*

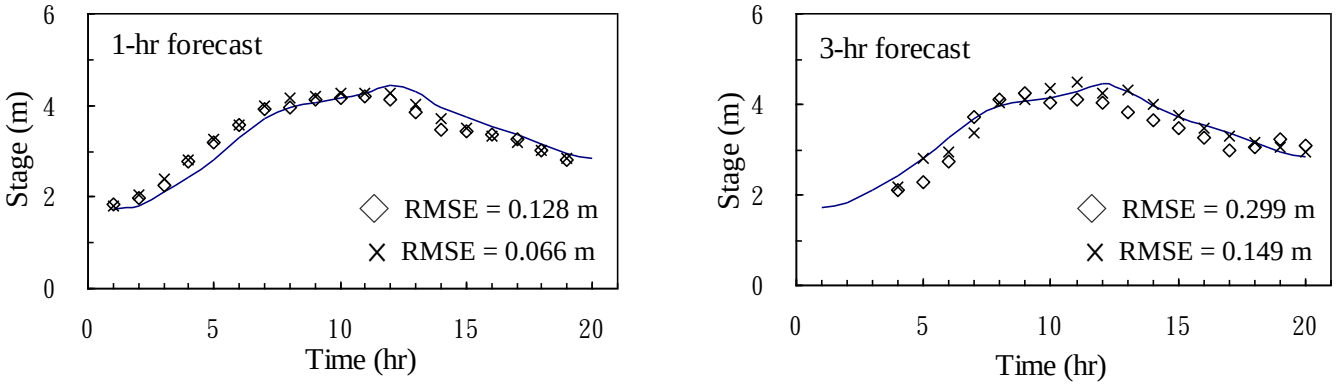

(a) Chungcheng Bridge

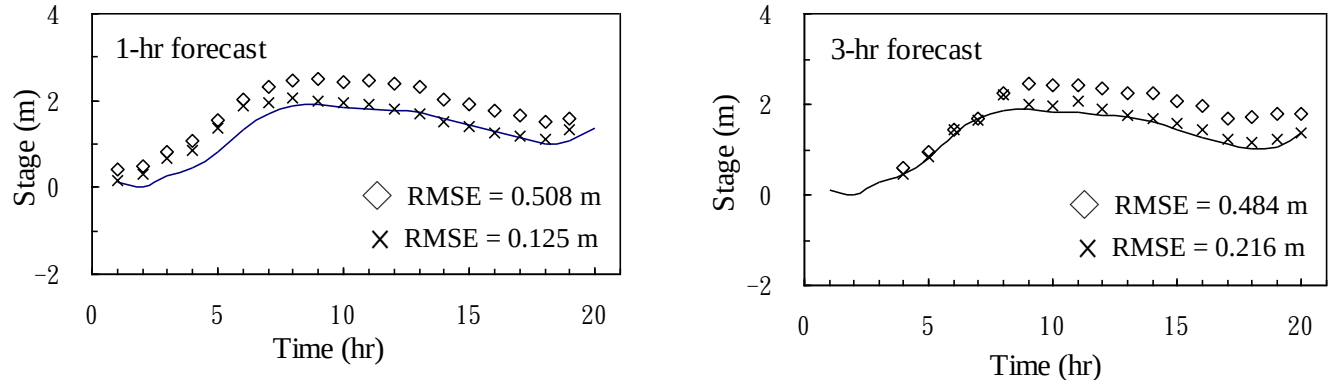

(b) Taipei Bridge

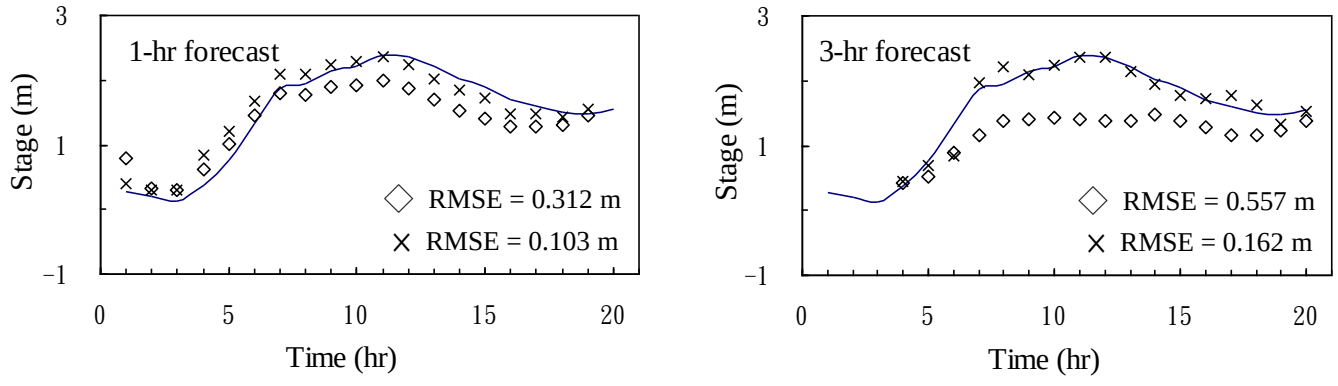

(c) Dazhi Bridge

Figure 7. The forecasted river stage hydrographs at the Chungcheng, Taipei, and Dazhi Bridge for Typhoon Haitang event.

Please cite as: *Hsu MH, Lin SH, Fu JC, Chung SF, Chen AS. (2010) Longitudinal stage profiles forecasting in rivers for flash floods, Journal of Hydrology, 388 (3-4), 426-437, DOI:10.1016/j.jhydrol.2010.05.028.*

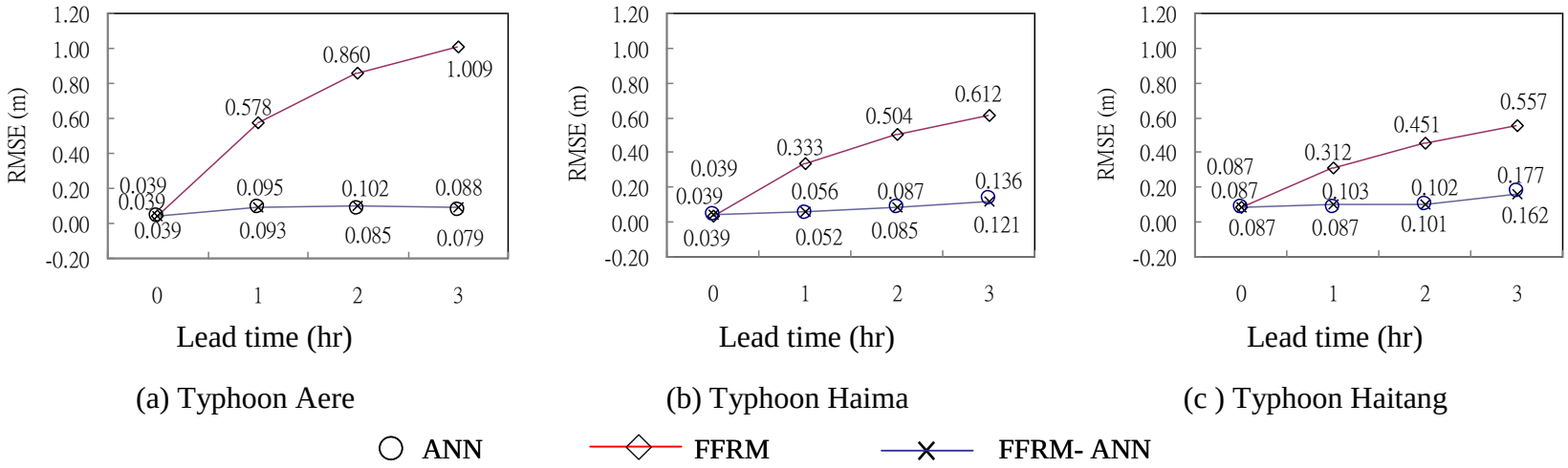

Figure 8.Model evaluation results for Typhoon Aere, Haima and Haitang events at Dazhi Bridge.

Please cite as: *Hsu MH, Lin SH, Fu JC, Chung SF, Chen AS. (2010) Longitudinal stage profiles forecasting in rivers for flash floods, Journal of Hydrology, 388 (3-4), 426-437, DOI:10.1016/j.jhydrol.2010.05.028.*

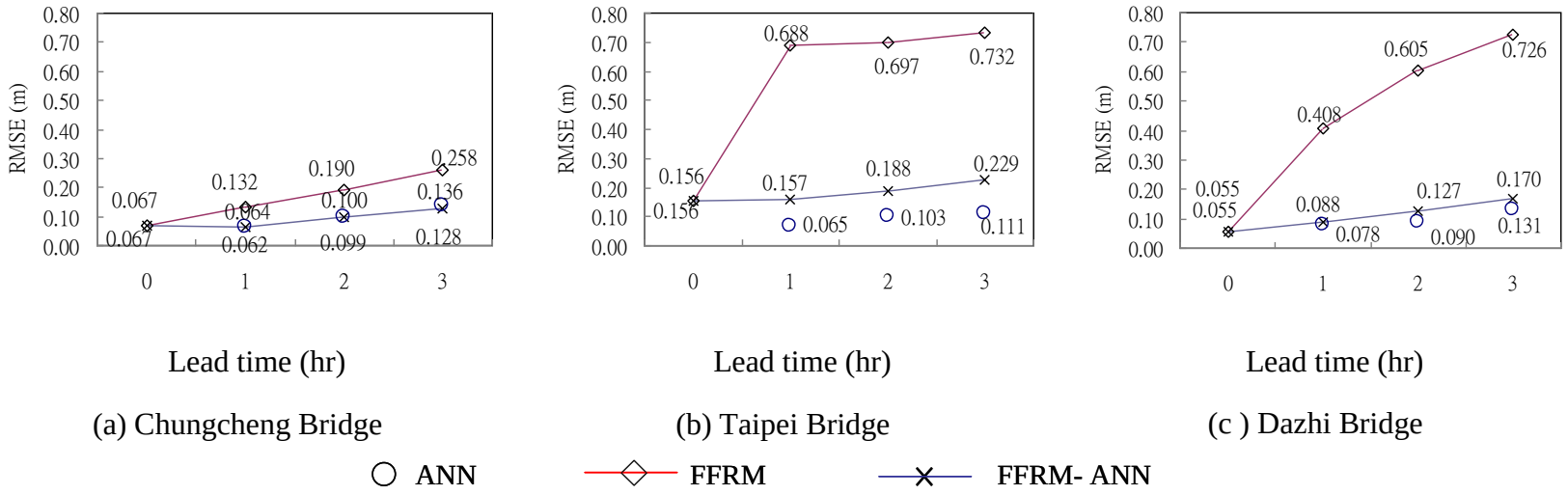

Figure 9. The mean RMSE at Chungcheng, Taipei and Dazhi Bridges for Typhoon Aere, Haima and Haitang evetns.

Please cite as: *Hsu MH, Lin SH, Fu JC, Chung SF, Chen AS. (2010) Longitudinal stage profiles forecasting in rivers for flash floods, Journal of Hydrology, 388 (3-4), 426-437, DOI:10.1016/j.jhydrol.2010.05.028.*

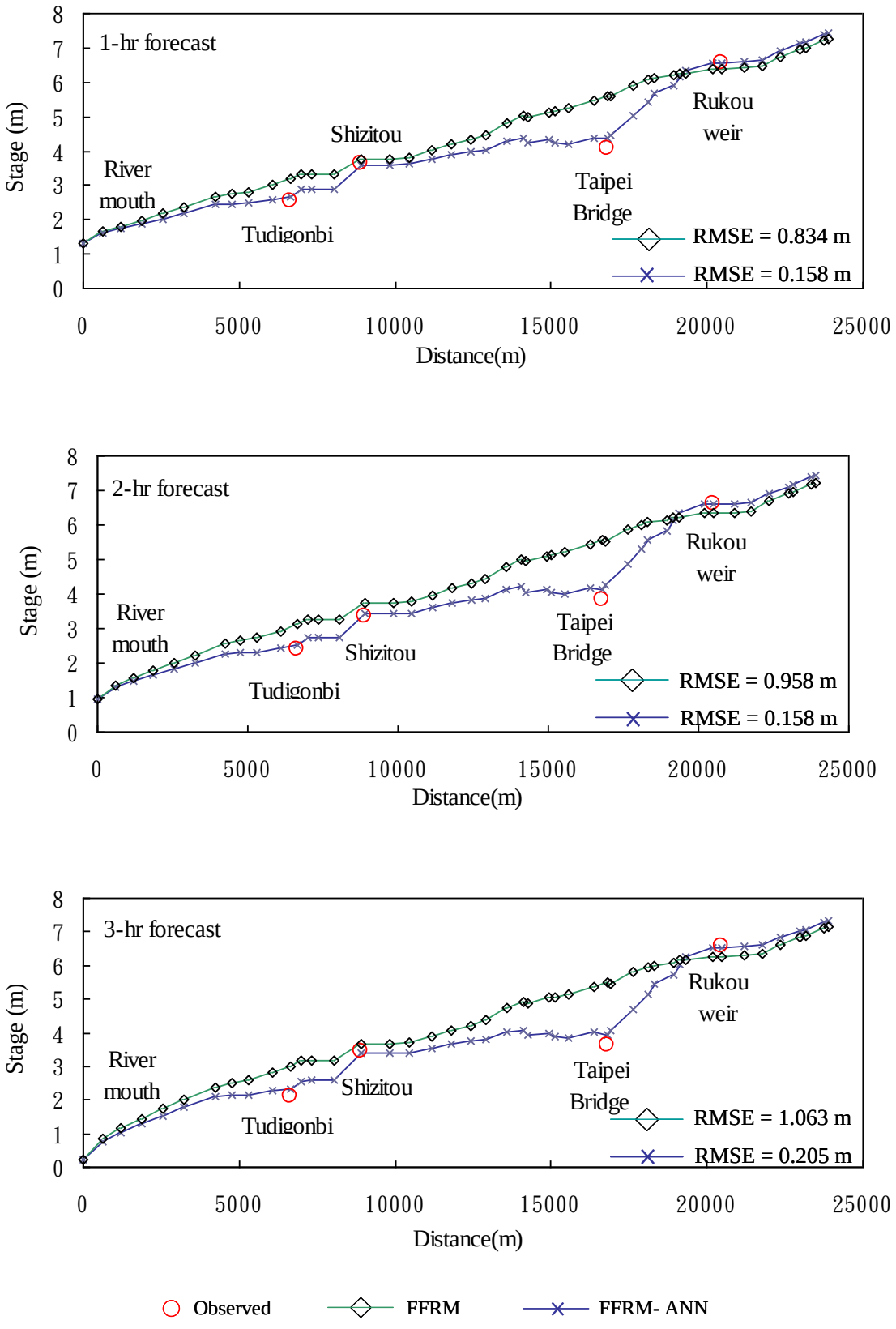

Figure 10. The forecasted peak stage profiles during Typhoon Aere event in the Tanshui River.

Please cite as: *Hsu MH, Lin SH, Fu JC, Chung SF, Chen AS. (2010) Longitudinal stage profiles forecasting in rivers for flash floods, Journal of Hydrology, 388 (3-4), 426-437, DOI:10.1016/j.jhydrol.2010.05.028.*

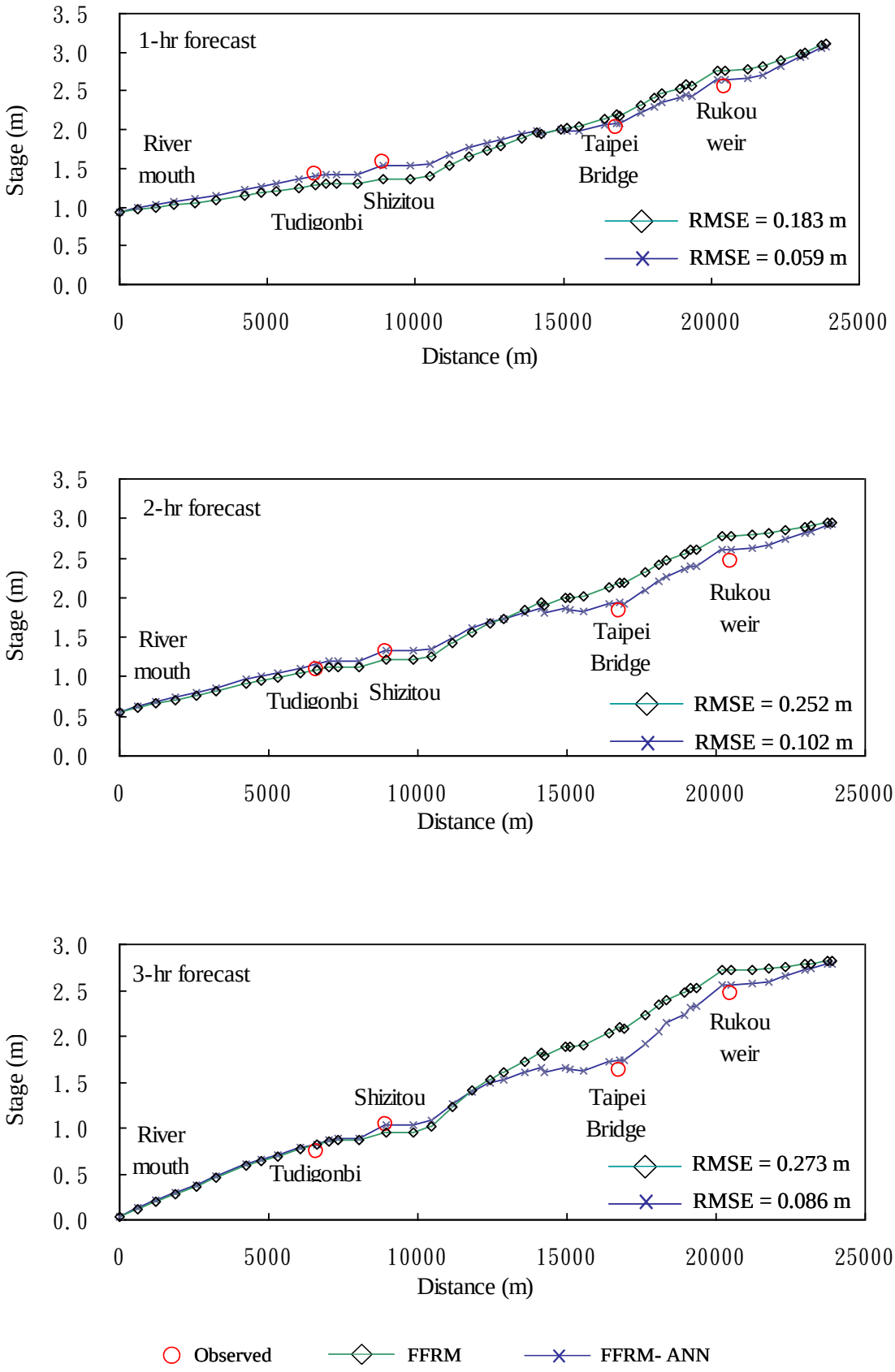

Figure 11. The forecasted peak stage profiles during Typhoon Haima event in the Tanshui River.

Please cite as: *Hsu MH, Lin SH, Fu JC, Chung SF, Chen AS. (2010) Longitudinal stage profiles forecasting in rivers for flash floods, Journal of Hydrology, 388 (3-4), 426-437, DOI:10.1016/j.jhydrol.2010.05.028.*

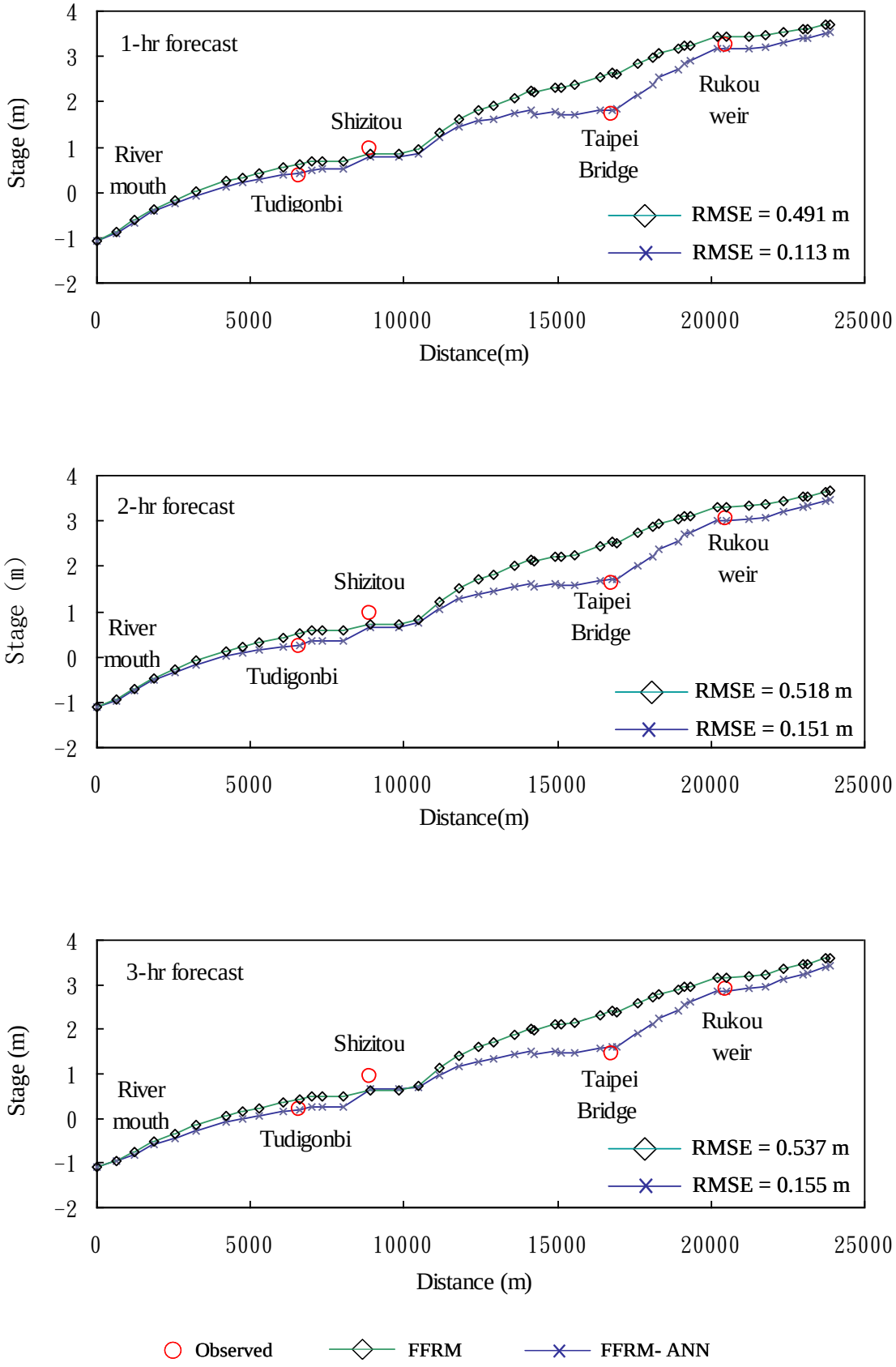

Figure 12. The forecasted peak stage profiles during Typhoon Haitang event in the Tanshui River.

Please cite as: *Hsu MH, Lin SH, Fu JC, Chung SF, Chen AS. (2010) Longitudinal stage profiles forecasting in rivers for flash floods, Journal of Hydrology, 388 (3-4), 426-437, DOI:10.1016/j.jhydrol.2010.05.028.*

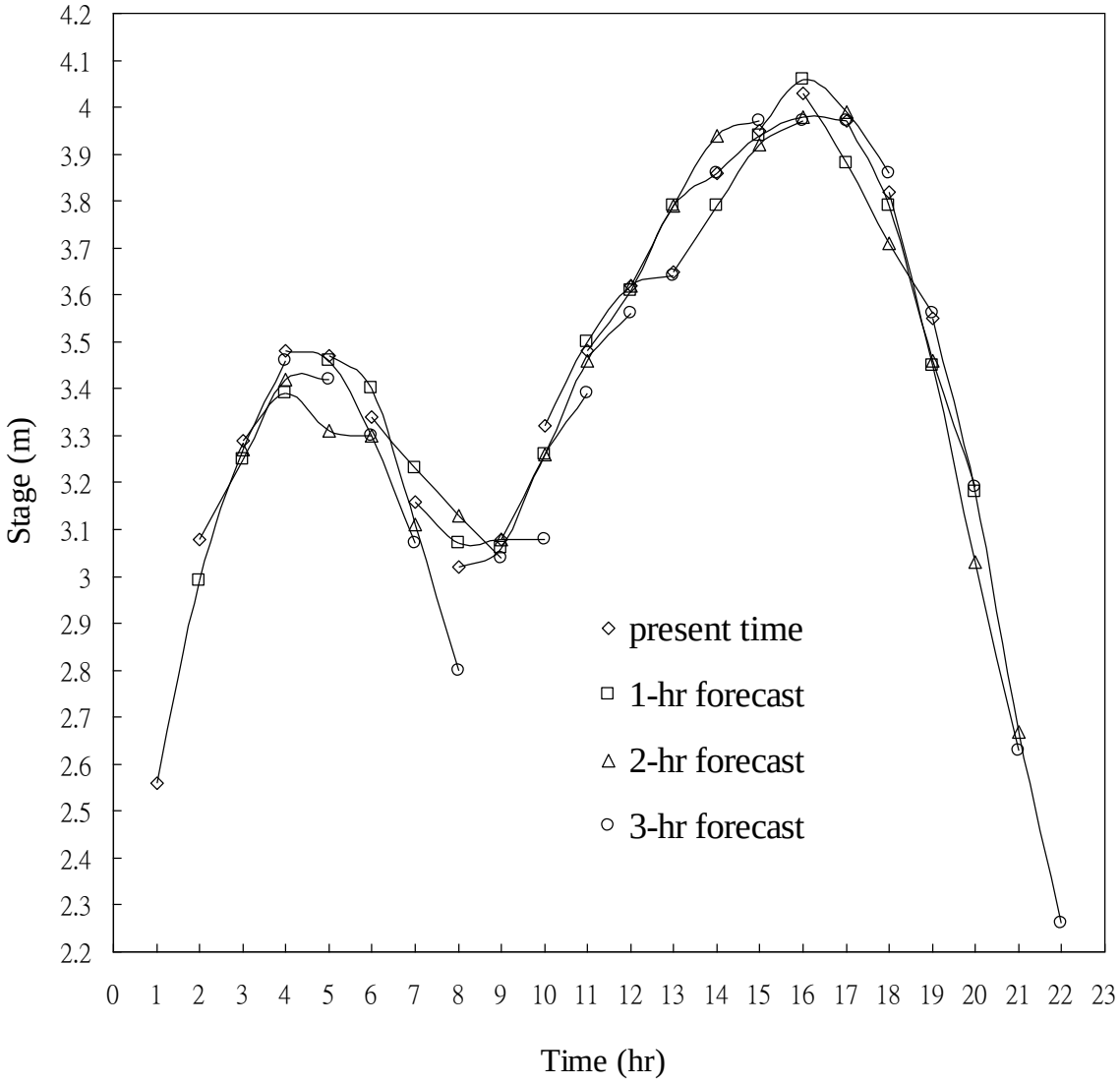

Figure 13.The forecasted stages at the Chungshan Bridge during typhoon Aere event.